https://doi.org/10.5194/egusphere-2025-2887
Preprint. Discussion started: 27 June 2025

30 years of total column ozone and aerosol optical depth measurements using the Brewer spectrophotometer in Poprad-Gánovce, Slovakia

Peter Hrabčák[1], Meritxell Garcia-Suñer[2], Violeta Matos[2], Víctor Estellés[2], Anna Pribullová[1], Jozef Depta[1], Martin Staněk[3], and Martin Stráník[3]

[1]Aerological and Solar Radiation Center, Slovak Hydrometeorological Institute, Gánovce, 058 01, Slovakia
[2]Department of Earth Physics and Thermodynamics, Universitat de València, Valencia, 46100, Spain
[3]Solar and Ozone Observatory, Czech Hydrometeorological Institute, Hradec Králové, 500 08, Czech Republic

Correspondence to: Peter Hrabčák (peter.hrabcak@shmu.sk)

Abstract. Long-term measurement series are a rare but valuable source of information. The first measurements using the Brewer ozone spectrophotometer in Slovakia began at the Poprad-Gánovce station in August 1993. As a result, a 30-year series of measurements was completed in 2023. The primary goal of this study is to present the calculated values of total column ozone (TCO) and aerosol optical depth (AOD) derived from measurements conducted with the same Brewer spectrophotometer. Additionally, this time series of measurements is enriched with tropopause height values, made possible by aerological sounding measurements regularly conducted at the Poprad-Gánovce station. This work provides a climatological and long-term trend analysis of the time series for these three atmospheric characteristics. The data used in this study are closely tied to three environmental issues driven by human activities: ozone depletion, climate change, and air pollution caused by aerosols. No clear trend was observed for the annual TCO averages, while AOD at 320 nm exhibited a distinct decresing trend with a slope of -0.06 per decade. The lowest annual average of AOD at 320 nm was measured in 2020, corresponding to the first year of the COVID-19 pandemic. The highest increases in tropopause height were found in August, at 200 m per decade, and in September, at 210 m per decade. The largest declines in TCO occurred in the same months, with a rate of change of -3.5 DU per decade in August and -2.8 DU per decade in September.

1 Introduction

Ozone depletion is caused by human-related emissions of ozone-depleting substances (ODSs) and the subsequent release of reactive halogen gases, particularly chlorine and bromine, in the stratosphere (WMO, 2022). Monitoring long-term changes in ozone, a vital component of Earth's atmosphere, is essential for assessing the effectiveness of the Montreal Protocol (UNEP, 2020). This protocol was established to regulate and significantly reduce the levels of persistent ODSs. Over the past two decades, measures implemented under the Montreal Protocol and its amendments have resulted in a substantial decline in the total concentration of ODSs (Braesicke et al., 2018). In addition to ODSs, model simulations indicate that stratospheric ozone concentrations are also influenced by the chemical and climatic effects of greenhouse gases. Specifically,

https://doi.org/10.5194/egusphere-2025-2887
Preprint. Discussion started: 27 June 2025

increasing concentrations of the greenhouse gases carbon dioxide (CO_2) and methane (CH_4) during this century are expected to raise global total column ozone (TCO) levels beyond the natural levels observed in the 1960s. This increase is primarily due to the cooling of the upper stratosphere and changes in stratospheric circulation. Conversely, the chemical effect of rising concentrations of nitrous oxide (N_2O), another greenhouse gas, is to deplete stratospheric ozone (WMO, 2022).

In the middle and high latitudes, the anticipated increase of TCO related to ODSs is obscured by significant dynamically induced interannual variability in ozone. Additionally, complex feedback mechanisms driven by climate change can result in further long-term variations in ozone levels, for instance, through changes in temperature (Coldewey-Egbers et al., 2022). According to Coldewey-Egbers et al. (2022), during the period 1995–2020, the middle latitudes of the Northern Hemisphere exhibited distinct regional trends, characterized by both latitudinal and longitudinal structures. Significant positive trends (1.5 ± 1.0 % per decade) were observed over the North Atlantic region, while barely significant negative trends (−1.0 ± 1.0 % per decade) were identified over Eastern Europe. Furthermore, these trends correlate with long-term changes in tropopause pressure.

The trend in tropopause altitude has been positive over recent decades at a global level, primarily driven by thermal effects due to the warming of the troposphere as a consequence of increasing greenhouse gas concentrations (Santer et al., 2003; Pisoft et al., 2021). For the European station Hohenpeißenberg, data from 1967 to 1997 revealed that approximately 25 % of the negative long-term trend in TCO could be attributed to a tropopause that rose by 150 ± 70 meters per decade (Steinbrecht et al., 1998). Positive correlations with the trend in ozone were found for the northern Pacific, for both the southern and northern parts of the North Atlantic, and for Europe according to Coldewey-Egbers et al. (2022). This study further states that the regions indicating a negative trend in ozone also show a negative trend in tropopause pressure with slopes between -3.0 and -3.5 hPa per decade during the period 1995–2020. The negative pressure trend corresponds to an increase of about 100–130 m per decade in tropopause height. On the other hand, the northern part of the North Atlantic indicates a positive trend both in ozone (1.2 ± 1.2 % per decade) and in tropopause pressure. The latter is about 2 hPa per decade in that region (Coldewey-Egbers et al., 2022).

It is well known that anthropogenic changes in TCO levels and atmospheric aerosols significantly impact the solar UV radiation reaching the Earth's surface (Kim et al., 2013; De Bock et al., 2014). It was found that the overall mean radiation amplification factor (RAF) due to TCO, RAF(AOD, SZA) (Madronich, 1993), shows that 1 % decrease in TCO results in an increase of 1.18 ± 0.02 % in the erythemal UV irradiance with the range of 0.67–1.74 % depending on solar zenith angles (SZAs) (40–70°) and on aerosol optical depths (AODs) (< 4.0), under both clear (cloud cover < 25 %) and all sky conditions. A similar analysis of the RAF(TCO, SZA) due to AOD under clear and all-sky conditions shows that on average, a 1 % increase in AOD forces a decrease of 0.29 ± 0.06 % in the erythemal UV irradiance with the maximum range 0.18–0.63 % depending on SZAs and TCO (Kim et al., 2013).

The study by Filonchyk et al. (2020) provides characteristics of aerosol columnar properties based on MODIS-Aqua measurements over ten countries in Eastern Europe (including Slovakia) from 2002 to 2019. A gradual reduction in AOD (at 550 nm) is observed in all countries, with decadal trends ranging from -0.050 (Belarus) to -0.029 (Russia). Slovakia is

https://doi.org/10.5194/egusphere-2025-2887
Preprint. Discussion started: 27 June 2025

characterized by a trend of -0.041 per decade. Results related to AOD at the Poprad-Gánovce station were previously published (Hrabčák, 2018). In that publication, data from 1994 to 2016 were analysed, representing a 23-year series of measurements. For the wavelength of 320 nm, the trend value was -0.05 ± 0.01 per decade. The following lines will update the information on the development of AOD at the Poprad-Gánovce location, as the series of measurements has already exceeded the 30-year milestone.

2 Methods

2.1 Location

The Brewer spectrophotometer is located on the roof of the Aerological and Solar Radiation Center in Poprad-Gánovce, part of the Slovak Hydrometeorological Institute. Its coordinates are 49.03° N, 20.32° E, at an altitude of 709 meters above sea level. The site is situated in the Podtatranská Basin, which forms part of the larger Carpathian geomorphological unit. The surrounding area includes mountain ranges of varying elevations. Gerlachovský štít (2654 m above sea level), the highest peak in the Carpathians, is only 20 km from the station. Local aerosol sources primarily include emissions from burning solid fuels, mainly wood, in nearby villages, as well as agricultural activities. The area experiences relatively strong winds when influenced by a larger pressure gradient, with prevailing wind directions from the west, north, and southeast.

The proximity of the city of Poprad, located approximately 1.5 kilometers away with a population of around 50 000 and various industrial activities, also influences the site. Despite its closeness to Poprad, the area is generally considered rural in terms of anthropogenic impact. Given that ozone is concentrated primarily in the stratosphere, local effects through ground-level ozone have only a minimal impact on its final value. The TCO above the measurement site at any time of the year depends almost exclusively on large-scale atmospheric circulation in the stratosphere.

2.2 Brewer ozone spectrophotometer

The Brewer ozone spectrophotometer (a single monochromator, model MKIV, No. 97) has been performing measurements at the Poprad-Gánovce station since 18 August 1993. It is a scientific instrument that operates in the ultraviolet and visible regions of the solar spectrum. The device enables measurements of the total vertical column of O_3, SO_2, and NO_2, as well as global UV radiation (from 290 nm to 325 nm, with a step of 0.5 nm). Using its optical system, the instrument decomposes solar radiation reaching the Earth's surface and selects predetermined wavelengths from the ultraviolet and visible parts of the spectrum, with stronger and weaker absorption by O_3, SO_2, and NO_2. Based on the differing absorption of radiation at these selected wavelengths, it is possible to derive the total amount of these gases in the vertical column of the atmosphere. Additionally, measurements of direct solar radiation can be used to determine the AOD.

Since the beginning of its operation, daily tests have been performed on the Brewer spectrophotometer using internal lamps, and it undergoes calibration every two years. The instrument is calibrated by International Ozone Services (IOS) Inc. against the global reference group (Brewer Triad), maintained by Environment Canada. The calibration is carried out during a

https://doi.org/10.5194/egusphere-2025-2887
Preprint. Discussion started: 27 June 2025

calibration campaign, usually on site or in a neighboring country, using a traveling reference instrument. From a technical perspective, the measurements can be considered homogeneous. The Brewer also enables the calculation of TCO using measurements of diffuse solar radiation. However, for the analysis of the TCO, only direct solar radiation measurements were used, as they are more accurate.

2.3 TCO calculation

The TCO data set consists of daily averages collected by the Brewer ozone spectrophotometer. These data cover the period from 18 August 1993 to 31 May 2024. All data used were derived from direct sunlight measurements obtained through the DS (direct sun) measurement procedure. A DS measurement is accepted only for an air mass factor of the ozone layer of less than 4 (as recommended by IOS), and it takes approximately 2.5 minutes. During this time, the density of solar radiation flux is measured five times for each of the five wavelengths. Consequently, five values of TCO in Dobson units (DU) are obtained from a single DS measurement, which are then used to calculate an average and a standard deviation. Only the measurements that meet the criterion (standard deviation ≤ 2.5 DU) are selected for further data analysis. The TCO was calculated using the Brewer spectrophotometer B data files analysis program v. 7.1 (O3Brewer) by Martin Stanek (http://www.o3soft.eu/; last access: February 2025). Brewer spectrophotometer data file (B-file) contains most of the raw data collected by the Brewer spectrophotometer.

2.4 AOD calculation

The Brewer spectrophotometer at the Poprad-Gánovce station allows for the determination of optical depth in the UV region of the spectrum at wavelengths of 306.3 nm, 310 nm, 313.5 nm, 316.8 nm, and 320 nm. The use of Brewer spectrophotometer measurements to determine AOD has been documented in numerous studies (e.g., Jarosławski et al., 2003; Kazadzis et al., 2007; López-Solano et al., 2018; Nuñez et al., 2023). In this study, the Langley plot method (LPM) was employed to calculate AOD. This traditional method is commonly used to calculate AOD from Brewer spectrophotometer data (Carvalho and Henriques, 2000; Nuñez et al., 2023). Notably, this method of AOD calculation has previously been applied to data from the Poprad-Gánovce site (Pribullová, 2002; Hrabčák, 2018).

This method requires stable atmospheric conditions to determine the extraterrestrial constants (ETCs) with sufficient accuracy. Specifically, low variability in TCO and AOD is essential during the measurement period. It is also necessary to avoid any cloud contamination in DS measurements and to ensure a sufficient range of zenith angles throughout the day, which is crucial for this method. Determining ETCs using the LPM at low-altitude stations in urbanized areas is not recommended unless corrections for the effects of diffuse radiation and the daily ozone cycle are known. This method is most suitable for lower latitudes (particularly in mountainous regions near the tropics) and has certain limitations in the middle and particularly higher latitudes (Marenco, 2007). Poprad-Gánovce is neither a typical low-altitude urbanized station nor a typical high-mountain site, rather it is situated between these two cases (Hrabčák, 2018).

https://doi.org/10.5194/egusphere-2025-2887
Preprint. Discussion started: 27 June 2025

The calculation of AOD is based on the theory described by the Beer-Bouguer-Lambert law. Applying this law to solar UV radiation passing through the atmosphere can be expressed as follows:

$$S_\lambda = S_{0,\lambda}\, e^{-\mu_w \tau_\lambda} = S_{0,\lambda}\, e^{-\mu_{O_3} \tau_{\lambda,O_3} - \mu_r \tau_{\lambda,r} - \mu_a \tau_{\lambda,a}}\,, \quad (1)$$

where S_λ is the flux density of solar radiation flow for the selected wavelength λ expressed by photon count per unit of time at the Earth's surface, $S_{0,\lambda}$ is the flux density of solar radiation flow for the selected wavelength expressed by photon count per unit of time above Earth's atmosphere (ETC). The total optical depth of atmosphere τ_λ consists of the optical depth for TCO τ_{λ,O_3}, the optical depth for Rayleigh scattering $\tau_{\lambda,r}$, and the AOD is denoted as $\tau_{\lambda,a}$, which is the parameter of interest. The contribution of sulfur dioxide was neglected mainly due to its low impact (Arola and Koskela, 2004) and the inaccurate determination at the Poprad-Gánovce station.

Furthermore, μ_{O_3} is the air mass factor of the ozone layer determined according to Evans and Komhyr (2008), μ_r is the air mass factor for Rayleigh scattering determined according to Kasten and Young (1989), μ_a is the air mass factor of aerosols ($\mu_a < 4$ for AOD). Due to the similar vertical profile of aerosols and water vapour, it holds that $\mu_a \cong \mu_{H_2O}$, where μ_{H_2O} is the air mass factor of water vapour determined according to Kasten (1966). The air mass factor for atmosphere as a whole μ_w was calculated as a weighted arithmetic average of individual aforementioned components, while the optical depth of a given component was the weighting factor.

2.4.1 TCO optical depth calculation

The TCO optical depth τ_{λ,O_3} was calculated for each accepted value of the TCO. The calculation is represented by the following equation:

$$\tau_{\lambda,O_3} = \Omega_{O_3}\, \alpha(\lambda,T) = \Omega_{O_3}\, \sigma(\lambda,T)\, n\,, \quad (2)$$

where Ω_{O_3} is the TCO in DU, and the next element $\alpha(\lambda,T)$, is the absorption coefficient for ozone, which can be further expressed as the product of $\sigma(\lambda,T)$, the effective absorption cross section of the ozone molecule (typically quantified for 1cm^2), and n, the molecule count given by 1 DU and 1cm^2. For ozone, this is a constant with the value n = 2.687 x 10^{16} DU^{-1} cm^{-2} (Schwartz and Warneck, 1995). Carlund et al. (2017) recommend utilizing the same effective absorption cross sections of the ozone molecule to calculate both the TCO and its optical depth, which are required to determine the AOD. The O3Brewer software utilizes the effective absorption cross sections of the ozone molecule, which are based on the measurements by Bass and Paur (1985). This scale is used to calculate the TCO within the Brewer spectrophotometer network, following the recommendations of the International Ozone Commission (http://www.esrl.noaa.gov/gmd/ozwv/dobson/papers/coeffs.html; last accessed: February 2025).

More recent and accurate values of effective absorption cross sections are now available based on measurements from the Molecular Spectroscopy Laboratory at the Institute of Environmental Physics (IUP), University of Bremen

https://doi.org/10.5194/egusphere-2025-2887
Preprint. Discussion started: 27 June 2025

(https://www.iup.uni-bremen.de/gruppen/molspec/databases/; last accessed: Febraury 2025; Gorshelev et al., 2014; Serdyuchenko et al., 2014). These values were used to calculate the TCO optical depth. To maintain consistency between the calculation of TCO optical depth and TCO, the TCO values (used exclusively for TCO optical depth calculations) were also calculated using the more recent set from the IUP. This calculation was performed following the recommendations of Redondas et al. (2014). The dependence of the effective absorption cross section on temperature is significant. An effective temperature is typically used for the given gas. In the case of ozone measurements using the Brewer spectrophotometer, a standard effective temperature of -45 °C (228.15 K) is defined (Redondas et al., 2014).

2.4.2 Rayleigh scattering optical depth calculation

The Rayleigh scattering optical depth $\tau_{\lambda,r}$ was calculated by the following equation:

$$\tau_{\lambda,r} = \beta(\lambda)\frac{P}{P_{std}}, \quad (3)$$

where element $\beta(\lambda)$ is the normalized optical depth for Rayleigh scattering under standard atmospheric pressure and for a vertical column, P is the atmospheric pressure at the observation site (an interpolation based on 3 daily measurements in local climatic terms was used), and P_{std} is the standard atmospheric pressure (101 325 Pa).

The normalized optical depth for Rayleigh scattering $\beta(\lambda)$ was calculated according to Bodhaine et al. (1999), specifically for the purpose of AOD calculation. The use of coefficients from Bodhaine et al. (1999) is consistent with the recommendations stated in the National Oceanic and Atmospheric Administration (NOAA) online document (https://www.esrl.noaa.gov/gmd/grad/neubrew/docs/RayleighInBrewer.pdf; last access: February 2025), which specifies that the standard coefficients used in the Brewer operating software must not be used to calculate the AOD. It is stated in Carlund et al. (2017) that the TCO calculated using the standard coefficients is higher compared to the use of coefficients according to Bodhaine et al. (1999). In view of the above and for the sake of consistency, the TCO values (only for the purpose of AOD calculation) were also determined using the coefficients from Bodhaine et al. (1999), instead of the standard coefficients.

2.4.3 Multistep raw data post-processing

The value of S_λ from Eq. (1) was obtained by adjustment of raw data (raw counts). The raw data cover the period from 18 August 1993 to 31 May 2024. It is essential to maintain the sequence of the following steps during their adjustment. In the first step, raw counts stored in a B-file were converted into count rates. In the second step, dead time compensation was applied. Both formulas are provided in the Brewer MKIV Spectrophotometer Operator's Manual (SCI-TEC Instruments Inc., 1999). After the dead time compensation, a correction for the stray-light effect was applied in the same manner as in Garane et al. (2006). The methodology of the given correction in the case of Brewer at the Poprad-Gánovce station is described in more detail in Hrabčák (2018).

https://doi.org/10.5194/egusphere-2025-2887
Preprint. Discussion started: 27 June 2025

In the fourth step, a correction for the temperature dependence was applied, including a spectral transmittance correction for the neutral density (ND) filter used (SCI-TEC Instruments Inc., 1999). These filters are automatically selected by the Brewer spectrophotometer based on the current solar radiation flux. There are five ND filters and five wavelengths, resulting in a total of 25 required attenuation values. The attenuation values for the filters are determined during the instrument's calibration. In the fifth step, the impact of polarization was compensated. The sixth and final step involved the correction for the impact of diffuse radiation on DS measurements following the recommendations of Arola and Koskela (2004). The methodology of this correction is described in more detail in Hrabčák (2018).

Applying the above criteria yields five initial values of S_λ from a single DS measurement, from which the five AODs is subsequently calculated. The final AOD for the given DS measurement is calculated as the arithmetic average of the five values. All final values of AOD underwent a quality control procedure, including cloud screening, according to Hrabčák (2018).

2.4.4 ETCs calculation

The ETC $S_{0,\lambda}$ for each wavelength was determined using the LPM. The LPM employs multiple measurements of direct solar radiation at different solar zenith angles. The key is to linearize Eq. (1) by applying the natural logarithm:

$$\ln(S_\lambda) = \ln(S_{0,\lambda}) - \mu_w \tau_\lambda \, . \tag{4}$$

For each measurement of direct solar radiation, there is one corresponding equation, where μ_w and $\ln(S_\lambda)$ are the known variables, while $\ln(S_{0,\lambda})$ and τ_λ are the unknowns. It is essential to linearly interpolate the obtained dependence of $\ln(S_\lambda)$ on μ_w using the least squares method. $\ln(S_{0,\lambda})$ is obtained when μ_w equals 0. The ETC for the given wavelength is valid for the entire intercalibration period, which is 2 years, consistent with the standard intercalibration period for ozone measurements. Neglected changes in the sensitivity of the instrument over shorter time periods represent a disadvantage of this method. It is assumed that any significant service modifications to the Brewer spectrophotometer during calibration may affect the calculation of both TOC and AOD. For this reason, a period not exceeding 2 years was used.

The methodology for calculating the ETCs is based on Hrabčák (2018); however, some of the points outlined below have been modified. The ETCs for individual wavelengths can be determined solely from DS measurements that meet the following three conditions:

1. The air mass factor for the atmosphere as a whole is less than 3.
2. The AOD calculated as an average of five values within a single DS measurement for the wavelength of 320 nm is less than 0.4.
3. The difference between the maximum and minimum value of AOD within a single DS measurement is less than 0.03.

Additionally, the ETCs were determined only for days that meet conditions 4 to 9:

4. The number of direct solar radiation measurements is at least 50 (i.e. 10 DS measurements).
5. The difference between the maximum and minimum air mass factor for the entire atmosphere is greater than 1.

https://doi.org/10.5194/egusphere-2025-2887
Preprint. Discussion started: 27 June 2025

6. The standard deviation from the measured values of the TCO on the given day is less than 3 DU.
7. The standard deviation from the measured AOD values on the given day is less than 0.04.
8. The following selection criteria were applied:

$$\left|\ln(S_\lambda)_i - \ln(S_\lambda)_j\right| < 1.75 * \frac{\sum_{i,j=1}^{n} \left|\ln(S_\lambda)_i - \ln(S_\lambda)_j\right|}{n}, \quad (5)$$

where $\ln(S_\lambda)_i$ is the value of $\ln(S_\lambda)$ obtained from the equation of linear interpolation after the substitution of a specific μ_w, $\ln(S_\lambda)_j$ is the actually measured value of $\ln(S_\lambda)$ at the given value of μ_w, and n is the total number of direct solar radiation measurements on the given day. The fundamental principle is to exclude measurements with residue values from the linear interpolation that are greater than or equal to 1.75 times the average residue on the given day. The threshold value of 1.75 in the above equation was selected based on the results of an optimization test. The aim of this test was to maximize the number of days with very good linear interpolation, where the selected days had to meet the ninth condition.

9. The determination coefficient for the linear interpolation is greater than 0.99.

In the end, the following criterion was applied to all determined ETCs within the given intercalibration period:

10. $$\frac{|ETC - AVERAGE(ETCs)|}{STDEV(ETCs)} < 1.5\,, \quad (6)$$

where $AVERAGE(ETCs)$ is the average of the determined ETCs and $STDEV(ETCs)$ is the standard deviation.

An average is calculated from the ETCs that meet the 10th criterion. At the beginning, initial values of AOD were not available. For this reason, it was not possible to apply the second and third criterion and it was also not possible to take into account the effect of aerosols in the calculation of μ_w and to determine the correction for the diffuse radiation. After the initial calculation, the entire process was applied in two iterations. The ETC varies around its mean value due to changes in the Earth–Sun distance. Its correction was carried out according to the recommendation of the Guide to Meteorological Instruments and Methods of Observation (WMO, 2008). This correction was recalculated and applied on a regular basis. The calculation of the apparent elevation and apparent zenith angle of the Sun was also performed according to the recommendations of the WMO (WMO, 2008). The apparent elevation of the Sun constitutes the fundamental principle in the calculation of air mass factor.

2.5 Tropopause data

The tropopause is defined as the natural boundary between the troposphere and the stratosphere, characterized by differences in temperature, potential vorticity, and chemical composition, particularly with regard to ozone and water vapor. It can be located at altitudes ranging from approximately 6 to 18 km, depending on the location and weather conditions. Data on the geopotential height (later only height) of the tropopause for the Poprad-Gánovce station were obtained through aerological measurements regularly conducted at the station at two standard times, 0 and 12 UTC. These data cover the period from 18 August 1993 to 31 May 2024. These measurements are carried out using the Vaisala radiosonde system. One of the primary

https://doi.org/10.5194/egusphere-2025-2887
Preprint. Discussion started: 27 June 2025

outputs of the measurements is the vertical temperature profile, which was used to determine the tropopause height. The tropopause is traditionally defined by meteorologists as the lowest level where the rate of temperature decrease with altitude (normally around 6 °C/km in the troposphere) drops to 2 °C/km, and in the next 2 km above this level, the temperature decrease never exceeds 2 °C/km.

2.6 Mann-Kendall test and Sen's slope estimator

Temporal trends in TCO, AOD, and tropopause height were analysed using the Mann-Kendall test (Mann, 1945; Kendall, 1975). This is one of the most widely used non-parametric tests for detecting trends in atmospheric variables, particularly useful when the dataset contains missing values, negative values, or measurements below detection limits. The Sen's slope estimator (Theil, 1950; Sen, 1968), also a non-parametric method, is closely related to the Mann-Kendall test, as it quantifies the magnitude of the trend. Sen's slope represents the overall trend of the entire time series and is computed as the median of the slopes calculated between all possible pairs of time points (Matos et al., 2025).

3 Results and discussion

3.1 Statistical characteristics of TCO and AOD

The analysed dataset consists of daily averages of TCO and AOD derived from direct sunlight measurements collected by the Brewer ozone spectrophotometer in Poprad-Gánovce. These data cover the period from 18 August 1993 to 31 May 2024. A total of five wavelength channels are available for AOD: 306.3 nm, 310 nm, 313.5 nm, 316.8 nm, and 320 nm, with the latter being the most accurate, as measurement uncertainty increases with decreasing wavelength. This is due to the increasing optical depth of TCO and Rayleigh scattering at shorter wavelengths (Hrabčák, 2018). For this reason, the 320 nm wavelength was preferred in the present statistical analyses of AOD.

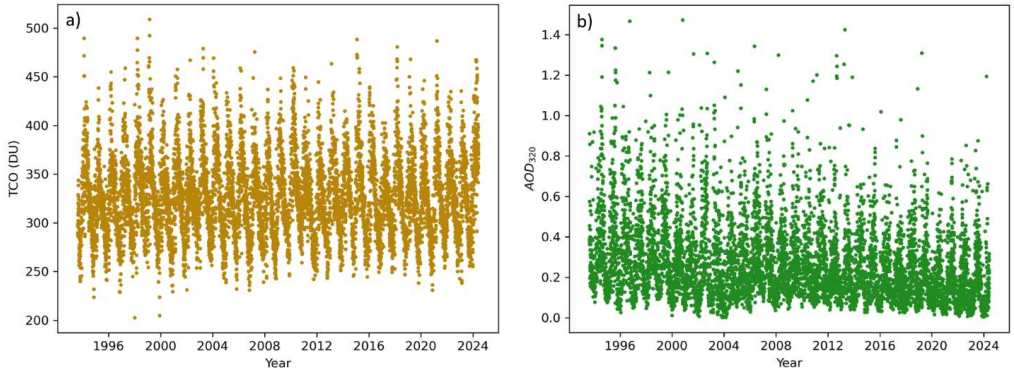

Figure 1 Daily mean values of TCO (a) and AOD_{320} (b) derived from measurements taken by the Brewer ozone spectrophotometer in Poprad-Gánovce from 18 August 1993 to 31 May 2024.

https://doi.org/10.5194/egusphere-2025-2887
Preprint. Discussion started: 27 June 2025

In this section, we present a study on the fundamental behaviour of TCO and AOD over time. The aim is to identify any patterns in these quantities that can be explained by atmospheric circulation or local aerosol emissions. To this end, the daily mean values of TCO and AOD at 320 nm (AOD_{320}) are plotted in Fig. 1. As observed, both quantities exhibit clear periodic behaviour. As shown in Fig. 1a, daily TCO averages vary over a relatively large range. The absolute lowest daily average TCO was recorded on 1 January 1998, with a value of 203 DU. Conversely, the highest daily average was observed on 24 February 1999, with a value of 509 DU. For AOD_{320}, all values equal to or greater than 1.5 were excluded during quality control.

The intra-annual variation of TCO and AOD_{320} has been analysed. For this purpose, several statistical parameters have been determined, including the median, mean, standard deviation, first and third quartiles, and minimum and maximum values for each month. The results are summarized in the boxplots in Fig. 2. Additionally, these statistics are presented in Table 1 and Table 2. These results are based on monthly means. Clear seasonal patterns are evident in both plots. The annual TCO cycle is more pronounced, with peak mean values occurring in March, followed by a decline to minimum values in October. The observed annual cycle is driven by the Brewer-Dobson circulation, which plays a key role in the global distribution of TCO (Rosenlof, 1995; Butchart et al., 2006).

TCO varies strongly with latitude over the globe, with the largest values occurring at middle and high latitudes during most of the year. This distribution is the result of the large-scale circulation of air in the stratosphere that slowly transports ozone rich air from high altitudes in the tropics, where ozone production from solar ultraviolet radiation is largest, toward the poles. Ozone accumulates at middle and high latitudes, increasing the vertical extent of the ozone layer and, at the same time, TCO. The TCO is generally smallest in the tropics for all seasons. An exception since the mid-1980s is the region of low values of ozone over Antarctica during spring in the Southern Hemisphere, a phenomenon known as the Antarctic ozone hole (Salawitch et al., 2023).

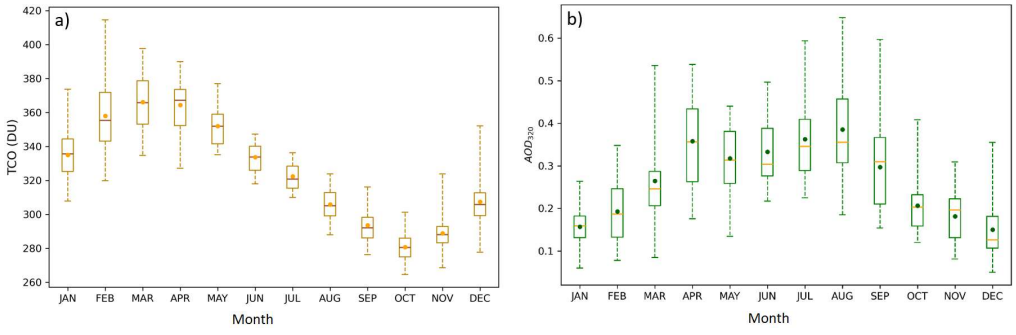

Figure 2 Boxplots showing the statistical distribution of TCO (a) and AOD_{320} (b) for each month based on data from September 1993 to May 2024. The means are represented by solid points. The horizontal lines inside the boxes indicate the medians. The boxes extend from the 25th percentile ($U25$) to the 75th percentile ($U75$). Additionally, the lower and upper whiskers represent the corresponding minimum and maximum values, respectively.

https://doi.org/10.5194/egusphere-2025-2887
Preprint. Discussion started: 27 June 2025

Table 1 Statistical parameters quantifying the inter-annual behavior of TCO based on data from September 1993 to May 2024. The second column represents the mean, the third the corresponding standard deviation, the fourth the median, followed by $U25$ and $U75$, which denote the 25th and 75th percentiles, respectively. N represents the number of days, and M the number of months with available data.

	$TCO\ (DU)$	$\sigma(TCO)(DU)$	$< TCO > (DU)$	$U25\ (DU)$	$U75\ (DU)$	N	M
January	335	17	336	325	344	665	31
February	358	20	355	343	372	673	31
March	366	16	366	353	379	801	31
April	364	16	367	352	374	808	31
May	352	12	352	342	359	831	31
June	334	8	334	326	340	819	30
July	322	8	321	315	328	873	30
August	306	9	305	299	313	853	31
September	294	11	292	286	298	784	31
October	281	9	281	275	286	763	31
November	289	11	288	283	293	647	31
December	307	15	306	299	313	572	31

TCO also varies with season. During spring, it exhibits maxima at latitudes poleward of about 45° N in the Northern Hemisphere and between 45° and 60° S in the Southern Hemisphere. These spring maxima are a result of increased transport of ozone from its source region in the tropics toward high latitudes during late autumn and winter. This poleward ozone transport is much weaker during the summer and early autumn periods and is weaker overall in the Southern Hemisphere (Salawitch et al., 2023). This natural seasonal cycle can be clearly observed in Fig. 2a. Furthermore, it has been reported that the Brewer-Dobson circulation seems to have accelerated during the last years due to the increased presence of greenhouse gases in the atmosphere (Braesicke et al., 2003; Butchart et al., 2006). Other natural atmospheric cycles (e.g., the Quasi-Biennial Oscillation, El Niño-Southern Oscillation, Arctic and Antarctic Oscillations, the solar cycle, etc.) have also been found to influence TCO (Coldewey-Egbers et al., 2022). Since these cycles operate on different timescales, assessing the individual impact of each on TCO is challenging.

Regarding the mean values of AOD_{320}, two peaks are typically observed throughout the year. The first occurs in April, while the second, more pronounced peak, appears in August. The April maximum may be related to the increased occurrence of dust intrusions from the Sahara, which are most frequent from April to June (Hrabčák, 2022). This effect is also found in other European sites in the period March to April (Garcia-Suñer et al., 2024). Additionally, anthropogenic spring biomass burning may also contribute. The highest AOD_{320} values during August may be related to characteristic sunny, light wind weather, which favor aerosol accumulation and more effective vertical mixing, increasing the boundary layer thickness. Moreover, due to higher summer irradiation and consequently increased evaporation, columnar water vapor (CWV) levels rise, favoring the growth of hygroscopic particles and thus increasing AOD_{320}. Additionally, higher irradiance promotes the formation of secondary aerosols. It is also important to take into account that the influence of local aerosol sources (natural

https://doi.org/10.5194/egusphere-2025-2887
Preprint. Discussion started: 27 June 2025

or anthropogenic) is not negligible during the warm half-year, when agricultural activities occur and pollen levels in the air increase.

Table 2 Statistical parameters quantifying the inter-annual behavior of AOD_{320} based on data from September 1993 to May 2024. The second column represents the mean, the third the corresponding standard deviation, the fourth the median, followed by $U25$ and $U75$, which denote the 25th and 75th percentiles, respectively. N represents the number of days, and M the number of months with available data.

	AOD_{320}	$\sigma(AOD_{320})$	$< AOD_{320} >$	$U25$	$U75$	N	M
January	0.16	0.05	0.16	0.13	0.18	456	31
February	0.19	0.07	0.19	0.13	0.25	474	31
March	0.26	0.09	0.25	0.21	0.29	608	31
April	0.36	0.11	0.36	0.26	0.43	628	31
May	0.32	0.08	0.31	0.26	0.38	669	31
June	0.33	0.08	0.30	0.28	0.39	682	30
July	0.36	0.09	0.35	0.29	0.41	728	30
August	0.39	0.11	0.36	0.31	0.46	733	31
September	0.30	0.10	0.31	0.21	0.37	642	31
October	0.21	0.07	0.20	0.16	0.23	606	31
November	0.18	0.06	0.20	0.13	0.22	461	31
December	0.15	0.07	0.13	0.11	0.18	387	31

The lower aerosol loading observed during the cold season can be attributed to various factors. On the one hand, during the cold half-year, a predominant westerly flow from the Atlantic Ocean is observed, bringing clean marine air masses. In addition, the station's higher-altitude location in a windy area prevents the accumulation of anthropogenic aerosols. Furthermore, the terrain surrounding the station is often wet or snow-covered during the cold seasons, which rules out the possibility of local dust sources.

3.2 Analysis of the trends in TCO and AOD

In this section, the time series of TCO and AOD_{320} over the years is analysed to determine the temporal evolution of these variables. As a first step, linear trends in the annual and seasonal means of TCO and AOD_{320} were determined to identify possible long-term changes. The data points were fitted using the linear regression method, which is used to draw conclusions about their behaviour. The next step is to apply a more advanced analysis: the Mann-Kendall test (Mann, 1945; Kendall, 1948; Gilbert, 1987), which assesses the statistical significance of the trend, and Sen's slope (Sen, 1968), which quantifies the magnitude of the increasing or decreasing trend.

The data for TCO and AOD_{320} were analysed by year and also by meteorological seasons. In this way, spring includes data from March to May; summer from June to August; autumn from September to November; and winter from December to February. Figures 3a and 3b show the corresponding linear fits, and Table 3 summarizes the values of the parameters

https://doi.org/10.5194/egusphere-2025-2887
Preprint. Discussion started: 27 June 2025

345 obtained from the fit for TCO and AOD_{320}. Due to shorter days, and a lower Sun elevation, fewer days with available measurements are observed during the cold half-year, especially from November to January. Therefore, to appropriately account for the contribution of each month, weighted means were used to calculate annual and seasonal averages. The weights were based on the number of calendar days in each month.

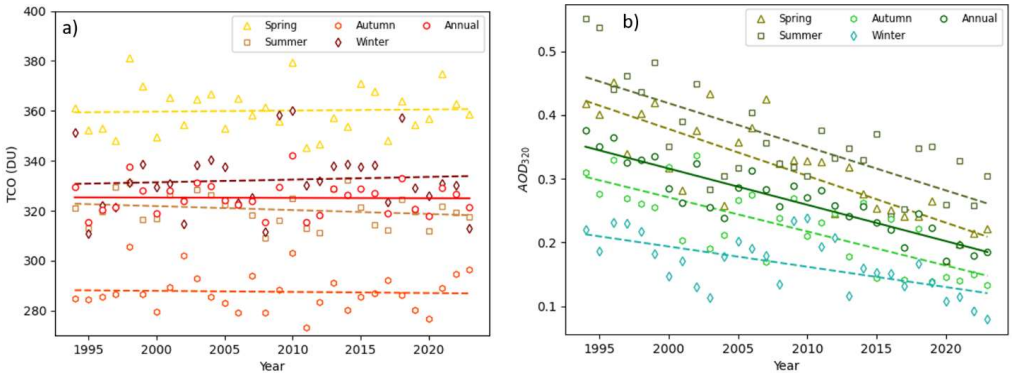

350 **Figure 3 Seasonal and annual trends in TCO (a) and AOD_{320} (b) based on data from 1994 to 2023, using linear regressions represented by dashed (seasonal) and solid (annual) lines, respectively. Triangles, squares, hexagons, and diamonds indicate the weighted means for spring, summer, autumn, and winter, respectively. Circles represent the weighted annual means.**

Figure 3a shows that the TCO does not follow any clear linear trend, with the exception of summer. On the other hand, 355 focusing on Fig. 3b, AOD_{320} clearly shows a decreasing trend across all seasons as well as in the annual data. As seen in Table 3, the R^2 values, which are indicators of the goodness of the fit, are quite small for TCO. In the case of AOD_{320}, these values are higher, as the corresponding means follow a clear decreasing trend. This descent is consistent with the analysis performed by Li et al. (2014), who detected a decreasing AOD trend in European countries. It is noteworthy that the lowest annual average of AOD_{320} was measured in 2020, during the first year of the COVID-19 pandemic.

360

Table 3 Parameters obtained from the linear regression analysis of seasonal and annual TCO and AOD_{320}, based on weighted means from 1994 to 2023.

	TCO		AOD_{320}	
	Trend (DU/decade)	**R^2**	**Trend ($decade^{-1}$)**	**R^2**
Spring	0.4	0.002	-0.07	0.69
Summer	-1.6	0.05	-0.07	0.57
Autumn	-0.4	0.002	-0.05	0.58
Winter	1.1	0.005	-0.03	0.39
Annual	-0.13	0.0003	-0.06	0.82

https://doi.org/10.5194/egusphere-2025-2887
Preprint. Discussion started: 27 June 2025

Our results are also consistent with the findings of Filonchyk et al. (2020), who, based on MODIS-Aqua measurements, reported a trend of −0.041 per decade in AOD_{550} over Slovakia during the period 2002–2019. This behaviour is primarily attributed to social and industrial changes in the Eastern European region. The key factors include the introduction of governmental policies to reduce anthropogenic pollutant emissions, the limitation of heavy industry, increased gasification, and public education.

Finally, Table 4 summarizes the results obtained from fitting the time evolution of AOD_{320} for each month of the year using the linear regression method. The trend is decreasing for all months. Furthermore, the trends for the months from March to September are steeper than those for the rest of the year. The results of the Mann-Kendall test and the corresponding values of Sen's slope have also been included in Table 4. It is worth noting that all months exhibit statistically significant AOD_{320} decreasing trends at least at the 95 % confidence level. Therefore, it can be concluded that AOD_{320} significantly decreases over the years. It is important to note the very good agreement found for each month between Sen's slope values and the slopes obtained from the linear regression analysis.

Table 4 Parameters (trends and R^2) obtained from the linear regression analysis of AOD_{320} for each month of the year, based on data from September 1993 to May 2024. In addition, results from the Mann-Kendall test are also included. Specifically, *Z* represents the test statistic of the Mann-Kendall test, and *S* denotes Sen's slope. *Z* values indicating statistically significant trends at the 95 % confidence level ($|Z| > 1.96$) have been highlighted in bold.

	Linear regression		Mann-Kendall test	
	Trend (decade^{-1})	R^2	Z	S (decade^{-1})
January	-0.02	0.16	**-2.2**	-0.02
February	-0.04	0.30	**-2.8**	-0.04
March	-0.07	0.42	**-4.2**	-0.06
April	-0.09	0.49	**-3.8**	-0.09
May	-0.07	0.57	**-4.6**	-0.07
June	-0.06	0.42	**-3.2**	-0.05
July	-0.06	0.33	**-3.1**	-0.06
August	-0.08	0.42	**-3.4**	-0.08
September	-0.07	0.36	**-3.6**	-0.07
October	-0.05	0.51	**-4.2**	-0.05
November	-0.04	0.41	**-3.1**	-0.04
December	-0.03	0.19	**-2.1**	-0.02

3.3 Analysis of the dependence of TCO on tropopause height

Several studies have focused on assessing the extent to which changes in TCO depend on variations in tropopause height (Steinbrecht et al. 1998, Varotsos et al. 2004, Coldewey-Egbers et al. 2022). In all mentioned studies, increasing trends have been found for tropopause height, while trends in TCO exhibit the opposite behaviour. In this section, the methodology used in Steinbrecht et al. (1998) and Varotsos et al. (2004) was applied to the data collected in Poprad-Gánovce. These studies

https://doi.org/10.5194/egusphere-2025-2887
Preprint. Discussion started: 27 June 2025

focused on locations in the Northern Hemisphere: Steinbrecht et al. (1998) in Hohenpeissenberg, Germany, and Varotsos et al. (2004) in Athens, Greece, so similar results can be expected for Poprad-Gánovce. However, the main difference between these studies and the present study is that measurements at Poprad-Gánovce cover the period from 1993 to 2024, whereas Steinbrecht et al. (1998) analysed data from 1967 to 1997, and Varotsos et al. (2004) from 1984 to 2002. Therefore, some differences are to be expected, especially in the trends of tropopause height and TCO.

Figure 4 shows the frequency distribution of the measured tropopause height values. The occurrence frequency is calculated by dividing the number of data points in each bin by the total number of data points. Each bin was defined as a half-open interval of height levels; for example, total ozone values contributing to the 8 km bin correspond to tropopause heights between 8.0 km (inclusive) and 9.0 km (exclusive). To account for the seasonality of the tropopause height, data corresponding to May/June/July and November/December/January (Nov/Dec/Jan) are plotted separately. Thus, it can be observed that the distribution for Nov/Dec/Jan is slightly wider than that for May/June/July.

This was also reported by Steinbrecht et al. (1998), who attributed it to more variable weather conditions in winter, which is likely to be the case for Poprad-Gánovce as well. Furthermore, as observed in these studies, the May/June/July distribution is shifted to higher altitudes. Indeed, the corresponding maximum occurs at 12 000 m, while for the Nov/Dec/Jan data, the maximum occurs at 11 000 m. Similar results were found in Athens by Varotsos et al. (2004), although they observed for May/June/July a secondary maximum at 16, 000 m, possibly due to the influence of tropical air.

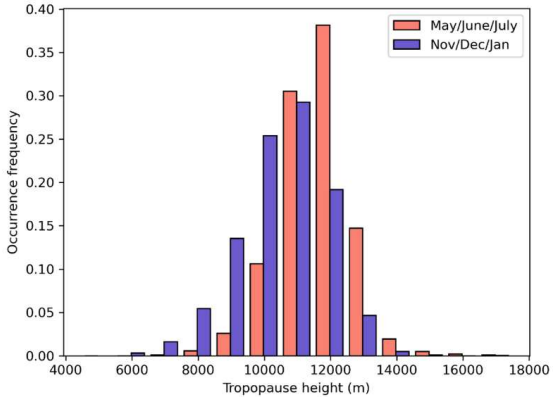

Figure 4 Occurrence frequency of tropopause heights for May/June/July (red) and November/December/January (purple) periods, based on measurements taken from 18 August 1993 to 31 May 2024.

When analyzing daily mean data, a clear anti-correlation between the two parameters can be observed: local minima in TCO correspond to maxima in tropopause height, and vice versa. This behavior is consistent with expectations for Eastern Europe (Coldewey-Egbers et al. 2022). To further investigate the relationship between TCO and tropopause height, the methodology used by Steinbrecht et al. (1998) was followed. Figure 5 shows mean TCO values for May/June/July and Nov/Dec/Jan, plotted separately as a function of tropopause height levels. The data used for the plot correspond to daily means between 18

https://doi.org/10.5194/egusphere-2025-2887
Preprint. Discussion started: 27 June 2025

August 1993 and 31 May 2024. The levels were defined in the same manner as in Fig. 4; for instance, tropopause height values at 8 km represent the mean of the TCO values measured for tropopause heights in the interval [8, 9) km, and so on. The points were fitted using linear regression analysis to parameterize their relationship.

Furthermore, the slope and R^2 values from the fit are provided in Table 5. The slopes are of the same order as those computed using data from Hohenpeissenberg and Athens. In fact, for the May/June/July period, Steinbrecht et al. (1998) reported a decrease in TCO of 16.3 DU/km in Hohenpeissenberg, while Varotsos et al. (2004) found that TCO decreases by 8.5 ± 0.7 DU/km in Athens. In Poprad-Gánovce, the decrease is 11.5 DU/km. On the other hand, the decrease is slightly steeper in the Nov/Dec/Jan period (11.7 DU/km). The magnitude of the May/June/July–Nov/Dec/Jan difference in TCO-tropopause height in Poprad-Gánovce is similar to that in Hohenpeissenberg, where a decrease of 15.7 DU/km was observed in Nov/Dec/Jan. Conversely, this difference is more significant in Athens, where the reported rate is -11.2 ± 0.5 DU/km for Nov/Dec/Jan. In any case, the slope is always negative, meaning that TCO decreases with the height of the tropopause.

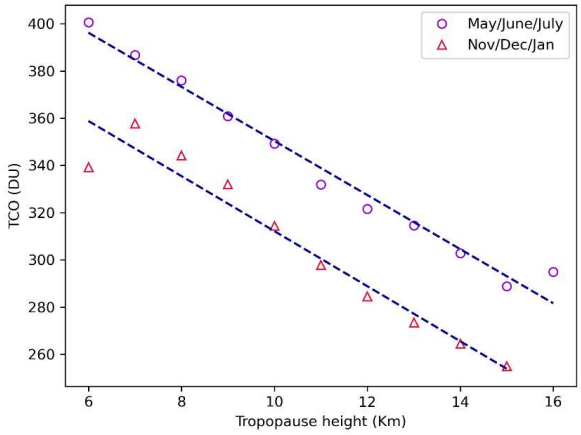

Figure 5 Linear fit of TCO means obtained for different ranges of tropopause height during the May, June, and July (purple) and November, December, and January (red) periods. The data set considered for the plot corresponds to days between 18 August 1993 and 31 May 2024, when daily means for both tropopause height and TCO are available.

Table 5 Parameters resulting from the linear regression analysis of TCO means computed for different ranges of tropopause height, based on data from 18 August 1993 to 31 May 2024.

Months	Slope (DU/km)	R^2
May/June/July	-11.5	0.98
Nov/Dec/Jan	-11.7	0.94

The temporal evolution of deseasonalized monthly running means of the TCO (ΔTCO) and tropopause height (Δh) time series over nearly 31 years of measurements is presented in Fig. 6a and 6b, respectively. Deseasonalization was achieved by computing the difference between each monthly mean and the long-term mean for the corresponding calendar month over

https://doi.org/10.5194/egusphere-2025-2887
Preprint. Discussion started: 27 June 2025

the period 1993–2024. The differences were next smoothed by applying a 13-month running mean. Hence, note that although data from September 1993 to May 2024 were available, running means can only be computed from March 1994 to November 2023.

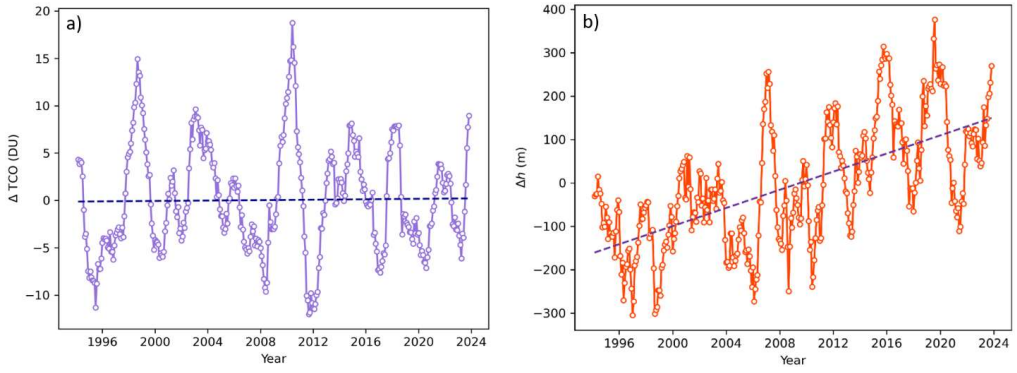

Figure 6 Representation of the time evolution of deseasonalized monthly running means of TCO (a) and tropopause height (b) from March 1994 to November 2023 (circles). Dashed lines represent linear fits to the data.

Next, linear regression was applied to the differences. The linear trend for ΔTCO is 0.11 DU per decade, and for Δh, it is 104 m per decade. Our results (particularly for ΔTCO) differ significantly from those reported by Steinbrecht et al. (1998) [ΔTCO = −10 DU/decade; Δh = 150 m/decade] and Varotsos et al. (2004) [ΔTCO = −7.5 ± 1.0 DU/decade; Δh = 167 ± 30 m/decade]. However, whereas Steinbrecht et al. (1998) analysed data from 1967–1997 and Varotsos et al. (2004) from 1984–2002, measurements in Poprad-Gánovce cover a more recent period (1994–2023). It is well known that various measures and regulations regarding the production of stratospheric ozone-depleting substances have been implemented to restore the ozone layer, most notably the Montreal Protocol in 1987 and its subsequent amendments. The effects of these actions have become evident in the halting of the TCO decline and the gradual recovery of TCO in recent years.

Following the investigations of Steinbrecht et al. (1998) and Varotsos et al. (2004), the linear relationship between TCO and tropopause height indicates a TCO decline of approximately −12 DU per 1 km increase in tropopause altitude. However, this relationship must be interpreted with caution when applied to different time periods. Indeed, several factors influence the relationship between TCO and tropopause height, including changes in the chemical composition of the atmosphere, which affect TCO, as well as stratospheric cooling and changes in the Brewer-Dobson circulation associated with climate change. The increase in tropopause height, primarily related to rising temperatures in the troposphere due to increased concentrations of greenhouse gases, contributes to ozone depletion by shifting the ozone layer to higher altitudes. This subsequently triggers photochemical processes that are enhanced at higher altitudes (Brasseur and Solomon, 1984), which in turn consume ozone and lead to a decrease in TCO (Steinbrecht et al., 1998). When applying the above-mentioned relationship between TCO and tropopause height, an increase in tropopause height of 104 m per decade would correspond to a decrease in TCO of

https://doi.org/10.5194/egusphere-2025-2887
Preprint. Discussion started: 27 June 2025

455 approximately −1.2 DU per decade. However, in reality, the TCO at Poprad-Gánovce does not follow this trend; instead, it shows a slight increase at a rate of 0.11 DU per decade (Fig. 6a).

Table 6 Parameters (trend and R^2) obtained from the linear regression analysis of tropopause height and TCO for each month of the year, based on data from January 1994 to December 2023. Additionally, results from the Mann-Kendall test are included. Specifically, *Z* represents the Mann-Kendall test statistic, and *S* denotes Sen's slope. *Z* values indicating statistically significant trends at a confidence level of at least 95 % ($|Z| > 1.96$) are highlighted in bold.

	Tropopause height				TCO			
	Linear regression		Mann-Kendall test		Linear regression		Mann-Kendall test	
Month	Trend (m/decade)	R^2	Z	S (m/decade)	Trend (DU/decade)	R^2	Z	S (DU/decade)
January	-60	0.02	-1.0	-112	4.6	0.06	1.2	4.1
February	67	0.01	0.8	105	-1.6	0.004	-0.5	-2.9
March	92	0.04	1.0	93	2.4	0.02	0.6	2.4
April	78	0.03	0.8	108	-2.6	0.02	-0.9	-2.7
May	-31	0.005	-0.4	-24	1.4	0.01	1.2	2.8
June	130	0.14	**2.2**	152	-0.4	0.002	-0.5	-0.7
July	120	0.08	1.6	146	-0.7	0.007	-0.5	-1.1
August	200	0.23	**2.9**	219	-3.5	0.12	-1.8	-4.0
September	210	0.14	**2.1**	251	-2.8	0.05	-1.4	-3.2
October	130	0.06	1.5	198	-0.7	0.005	0.1	0.3
November	150	0.09	1.9	188	2.3	0.03	1.0	1.9
December	90	0.02	0.7	68	0.03	$3 \cdot 10^{-6}$	-0.07	-0.3

Although no clear impact of the increasing trend in tropopause height on TCO is evident in the deseasonalized monthly running means, distinct variations are observed in certain months. The temporal evolution of the monthly mean TCO and 465 tropopause height has been analysed using linear regression. The corresponding results are summarized in Table 6, in a manner similar to those presented in Table 4 for AOD_{320}. Although not all months exhibit the expected behavior (e.g., January and May for tropopause height), it is important to notice that for the best fits (i.e., those with higher associated values of R^2) the expected trend is found.

The Mann-Kendall test was also applied to analyse trends in the monthly data. It is worth noting that the slopes determined 470 from the linear fits are very similar to the Sen's slopes, confirming the consistency between the two methods. Significant increasing trends in tropopause height at a confidence level of at least 95 % have been found in June, August, and September. The most significant decreasing trends in TCO were identified in August and September. It is precisely in the case of these two months that it can be argued that the observed decreasing trend in TCO is likely caused by a significant increase in tropopause height. The decreasing trend in TCO in April may be primarily related to anthropogenic stratospheric 475 ozone depletion. Episodes of unusually low TCO values were observed in April 2011 and 2020, following exceptionally cold and prolonged stratospheric winters, characterized by a strong and persistent Arctic polar vortex (Manney et al., 2020). On

https://doi.org/10.5194/egusphere-2025-2887
Preprint. Discussion started: 27 June 2025

the other hand, in the case of January, the increasing TCO trend shows, in addition to the weakening influence of halogen gases and a slight decrease in tropopause height, signs of a potential acceleration of the Brewer-Dobson circulation, which is the most active during the local winter.

4 Conclusions

This study summarizes the results obtained from the climatological analysis of over 30 years (18 August 1993 – 31 May 2024) of TCO and AOD data collected by a Brewer ozone spectrophotometer installed at the Poprad-Gánovce station in Slovakia. In particular, the intra-annual behaviour and the evolution of the annual, seasonal, and monthly means over the years have been analysed. The analysis found that both parameters exhibit seasonal patterns. On the one hand, AOD_{320} exhibits two distinct peaks during the warm half-year. The peak in April may be related to Saharan dust intrusions and spring biomass burning, while the one in August could be associated with summer conditions that favour particle accumulation, growth, and the formation of secondary aerosols. For TCO, higher levels are observed from February to April. This is related to the Brewer-Dobson circulation process.

Regarding temporal trends, the obtained results are in good agreement with the broader context of recent atmospheric developments in Eastern Europe. No clear trend has been identified for the annual averages of TCO, while AOD_{320} has shown a distinct decreasing trend over the years, with a value of -0.06 per decade. This is consistent with other studies in Europe (Li et al., 2014; Filonchyk et al., 2020; Garcia-Suñer et al., 2024). It is noteworthy that the decreasing trend in AOD_{320} is statistically significant in all months of the year. The explanation lies in the social and industrial changes in the region that have caused a significant decrease in anthropogenic air pollution. It is important to note that the lowest annual average of AOD_{320} was measured in 2020, during the first year of the COVID-19 pandemic.

Finally, the relationship between TCO and tropopause height has been examined. Unlike TCO, which exhibits a very small overall linear trend of 0.11 DU per decade, the trend for tropopause height is substantially higher at 104 m per decade. Long-term changes in individual months of the year reveal specific trends. The highest increasing linear trends in tropopause height have been found in August, reaching 200 m per decade, and in September, reaching 210 m per decade. The highest declining trend in TCO was recorded in the same two months. In August, it is -3.5 DU per decade, and in September, it is -2.8 DU per decade. We assume that the observed decreasing trend in TCO during these two months is likely driven by a significant rise in tropopause height.

The April decrease in TCO is likely linked to anthropogenic ozone depletion, with exceptionally low values recorded in 2011 and 2020 after unusually cold and prolonged winters associated with a strong stratospheric Arctic polar vortex (Manney et al., 2020). In contrast, for January, the increasing TCO trend suggests indications of a potential acceleration in the Brewer-Dobson circulation, which is most active during winter. It can be stated that atmospheric changes due to increasing greenhouse gas concentrations are likely beginning to manifest their impacts on TCO, but in different ways across individual months of the year. In conclusion, it can be stated that while the negative impact of halogen gases is gradually

https://doi.org/10.5194/egusphere-2025-2887
Preprint. Discussion started: 27 June 2025

weakening, the influence of climate change on TCO is increasing. Therefore, continuing regular measurements of TCO is necessary.

Code availability

The Python code for calculating the AOD is available from the corresponding author upon reasonable request.

Data availability

The data used in this study are available from the corresponding author upon reasonable request.

Author contributions

PH developed the initial concept of the study, calculated the AOD, and coordinated the work. MGS and VM performed the data analysis and contributed to the preparation of the manuscript. AP and VE contributed to the editing of the manuscript. JD was responsible for the acquisition of aerological measurement data. MS was in charge of the calibration of the Brewer spectrophotometer and the development of O3Brewer software. MS supported cooperation between the Czech and Slovak hydrometeorological institutes.

Competing interests

The authors have no competing interests to declare.

Acknowledgments

We would like to express our sincere gratitude to all current and former colleagues who contributed to ensuring the measurements at the Poprad-Gánovce station.

Financial support

This work was supported both from COST Action CA21119 Harmonia: International network for harmonisation of atmospheric aerosol retrievals from ground based photometers, supported by COST (European Cooperation in Science and Technology). Participation of M. Garcia-Suñer and V. Matos was made possible respectively by grant PREP2022-000658 from the Spanish Science and Innovation Ministry, and project PID2022-138730OB-I00, funded by the Spanish Ministry of Economy and Competitiveness and the European Regional Development Fund.

https://doi.org/10.5194/egusphere-2025-2887
Preprint. Discussion started: 27 June 2025

References

Arola, A. and Koskela, T.: On the sources of bias in aerosol optical depth retrieval in the UV range, J. Geophys. Res., 109, D08209, https://doi.org/10.1029/2003JD004375, 2004.

Bass, A. M. and Paur, R. J.: The ultraviolet cross-sections of ozone. I. The measurements, II. Results and temperature dependence, in: Atmospheric ozone, Proceedings of the Quadrennial ozone symposium, 3–7 September 1984, Halkidiki, Greece, 606–616, 1985.

Bodhaine, B. A., Wood, N. B., Dutton, E. G., and Slusser, J. R.: On Rayleigh Optical Depth Calculations, J. Atmos. Ocean. Tech., 16, 1854–1861, 1999.

Braesicke, P. and Pyle, J. A.: Changing ozone and changing circulation in northern mid-latitudes: Possible feedbacks?, Geophys. Res. Lett., 30, 1059, https://doi.org/10.1029/2002GL015973, 2003.

Braesicke, P., Neu, J., Fioletov, V., Godin-Beekmann, S., Hubert, D., Petropavlovskikh, I., Shiotani, M., and Sinnhuber, B. M.: Update on global ozone: Past, present, and future, in: Scientific Assessment of Ozone Depletion: 2018, Chap. 3, Global Ozone Research and Monitoring Project – Report No. 58, World Meteorological Organization, Geneva, Switzerland, 2018. Available at: https://ozone.unep.org/sites/default/files/2019-05/SAP-2018-Assessment-report.pdf

Brasseur, G. P. and Solomon, S.: Aeronomy of the Middle Atmosphere: Chemistry and Physics of the Stratosphere and Mesosphere, 441 pp., D. Reidel, Norwell, Mass., 1984.

Butchart, N., Scaife, A. A., Bourqui, M., et al.: Simulations of anthropogenic change in the strength of the Brewer–Dobson circulation, Clim. Dynam., 27, 727–741, https://doi.org/10.1007/s00382-006-0162-4, 2006.

Carlund, T., Kouremeti, N., Kazadzis, S., and Gröbner, J.: Aerosol optical depth determination in the UV using a four-channel precision filter radiometer, Atmos. Meas. Tech., 10, 905–923, https://doi.org/10.5194/amt-10-905-2017, 2017.

Carvalho, F. and Henriques, D.: Use of Brewer ozone spectrophotometer for aerosol optical depth measurements on ultraviolet region, Adv. Space Res., 25, 997–1006, 2000.

Coldewey-Egbers, M., Loyola, D. G., Lerot, C., and Van Roozendael, M.: Global, regional, and seasonal analysis of total ozone trends derived from the 1995–2020 GTO-ECV climate data record, Atmos. Chem. Phys., 22, 6861–6878, https://doi.org/10.5194/acp-22-6861-2022, 2022.

De Bock, V., De Backer, H., Van Malderen, R., Mangold, A., and Delcloo, A.: Relations between erythemal UV dose, global solar radiation, total ozone column and aerosol optical depth at Uccle, Belgium, Atmos. Chem. Phys., 14, 12251–12270, https://doi.org/10.5194/acp-14-12251-2014, 2014.

Evans, R. and Komhyr, W.: Operations handbook – Ozone observations with a Dobson spectrophotometer (WMO/GAW Report No. 183), World Meteorological Organization, Geneva, Switzerland, 2008.

Filonchyk, M., Hurynovich, V., and Yan, H.: Trends in aerosol optical properties over Eastern Europe based on MODIS-Aqua, Geosci. Front., 11, 2169–2181, https://doi.org/10.1016/j.gsf.2020.03.014, 2020.

https://doi.org/10.5194/egusphere-2025-2887
Preprint. Discussion started: 27 June 2025

Garane, K., Bais, A. F., Kazadzis, S., Kazantzidis, A., and Meleti, C.: Monitoring of UV spectral irradiance at Thessaloniki (1990– 2005): data re-evaluation and quality control, Ann. Geophys., 24, 3215–3228, https://doi.org/10.5194/angeo-24-3215-2006, 2006.

Garcia-Suñer, M., Matos, V., Kumar, G., Estellés, V., and Utrillas, M. P.: 20 years of columnar aerosol properties at Valencia area (Eastern Spain) by ground-based sun-photometry, Atmos. Res., 300, 107198, https://doi.org/10.1016/j.atmosres.2023.107198, 2024.

Gilbert, R. O.: Statistical Methods for Environmental Pollution Monitoring, Wiley, New York, 1987. Available at: https://www.osti.gov/biblio/7037501

Gorshelev, V., Serdyuchenko, A., Weber, M., Chehade, W., and Burrows, J. P.: High spectral resolution ozone absorption crosssections – Part 1: Measurements, data analysis and comparison with previous measurements around 293 K, Atmos. Meas. Tech., 7, 609–624, https://doi.org/10.5194/amt-7-609-2014, 2014.

Hrabčák, P.: Comparison of the optical depth of total ozone and atmospheric aerosols in Poprad-Gánovce, Slovakia, Atmos. Chem. Phys., 18, 7739–7755, https://doi.org/10.5194/acp-18-7739-2018, 2018.

Hrabčák, P.: Saharan dust over Slovakia in the years 2015–2020, Meteorol. J., 25, 3–15, 2022. Available at: https://www.shmu.sk/File/ExtraFiles/MET_CASOPIS/1658950036_MC_2022-1.pdf

Jarosławski, J., Krzyscin, J. W., Puchalski, S., and Sobolewski, P.: On the optical thickness in the UV range: Analysis of the groundbased data taken at Belsk, Poland, J. Geophys. Res., 108, 4722, https://doi.org/10.1029/2003JD003571, 2003.

Kasten, F.: A new table and approximation formula for the relative optical air mass, Arch. Meteor. Geophy. B, 14, 206–223, 1966.

Kasten, F. and Young, A. T.: Revised optical air mass tables and approximation formula, Appl. Optics, 28, 4735–4738, 1989.

Kazadzis, S., Bais, A., Amiridis, V., Balis, D., Meleti, C., Kouremeti, N., Zerefos, C. S., Rapsomanikis, S., Petrakakis, M., Kelesis, A., Tzoumaka, P., and Kelektsoglou, K.: Nine years of UV aerosol optical depth measurements at Thessaloniki, Greece, Atmos. Chem. Phys., 7, 2091–2101, https://doi.org/10.5194/acp7-2091-2007, 2007.

Kendall, M. G.: Rank Correlation Methods, 4th Edn., Charles Griffin, London, 1975.

Kim, J., Cho, H.-K., Mok, J., Yoo, H. D., and Cho, N.: Effects of ozone and aerosol on surface UV radiation variability, J. Photoch. Photobio. B, 119, 46–51, https://doi.org/10.1016/j.jphotobiol.2012.11.007, 2013.

Li, J., Carlson, B. E., Dubovik, O., and Lacis, A. A.: Recent trends in aerosol optical properties derived from AERONET measurements, Atmos. Chem. Phys., 14, 12271–12289, https://doi.org/10.5194/acp-14-12271-2014, 2014.

López-Solano, J., Redondas, A., Carlund, T., Rodriguez-Franco, J. J., Diémoz, H., León-Luis, S. F., Hernández-Cruz, B., Guirado-Fuentes, C., Kouremeti, N., Gröbner, J., Kazadzis, S., Carreño, V., Berjón, A., Santana-Díaz, D., Rodríguez-Valido, M., De Bock, V., Moreta, J. R., Rimmer, J., Smedley, A. R. D., Boulkelia, L., Jepsen, N., Eriksen, P., Bais, A. F., Shirotov, V., Vilaplana, J. M., Wilson, K. M., and Karppinen, T.: Aerosol optical depth in the European Brewer Network, Atmos. Chem. Phys., 18, 3885–3902, https://doi.org/10.5194/acp-18-3885-2018, 2018.

https://doi.org/10.5194/egusphere-2025-2887
Preprint. Discussion started: 27 June 2025

Madronich, S.: The atmosphere and UV-B radiation at ground level, in: Environmental UV Photobiology, edited by: Young, A. R., Björn, L. O., Moan, J., and Nultsch, W., Springer US, Boston, MA, 1–39, 1993.

Mann, H. B.: Nonparametric tests against trend, Econometrica, 13, 245–259, https://doi.org/10.2307/1907187, 1945.

Manney, G. L., Santee, M. L., Lawrence, Z. D., Lambert, A., and Livesey, N. J.: Record-low Arctic stratospheric ozone in 2020: MLS observations and comparisons with previous extreme winters, Geophys. Res. Lett., 47, e2020GL089063, https://doi.org/10.1029/2020GL089063, 2020.

Marenco, F.: On Langley plots in the presence of a systematic diurnal aerosol cycle centered at noon: A comment on recently proposed methodologies, J. Geophys. Res., 112, D06205, https://doi.org/10.1029/2006JD007248, 2007.

Matos, V., Sorribas, M., Segura, S., Utrillas, M. P., and Estellés, V.: Long-term (2011–2023) analysis of traffic and biomass burning contributions to black carbon in the third largest metropolitan area of Spain, Atmos. Pollut. Res., 16, 102527, https://doi.org/10.1016/j.apr.2025.102527, 2025.

Nuñez, M., Serrano, A., and Larson, N. R.: A climatology of aerosol optical depths in the ultraviolet wavelengths for Hobart, Australia, as determined by a Brewer MKIII spectrophotometer, Int. J. Climatol., 43, 632–649, https://doi.org/10.1002/joc.7802, 2023.

Pisoft, P., Sacha, P., Polvani, L. M., Añel, J. A., de la Torre, L., Eichinger, R., Foelsche, U., Huszar, P., Jacobi, C., Karlicky, J., Kuchar, A., Miksovsky, J., Zak, M., and Rieder, H. E.: Stratospheric contraction caused by increasing greenhouse gases, Environ. Res. Lett., 16, 064038, https://doi.org/10.1088/1748-9326/abfe2b, 2021.

Pribullová, A.: Spectral UV aerosol optical thickness determinated from the Poprad-Gánovce Brewer spectrophotometer observations, Contrib. Geophys. Geodesy., 32, 291–307, 2002.

Redondas, A., Evans, R., Stuebi, R., Köhler, U., and Weber, M.: Evaluation of the use of five laboratory-determined ozone absorption cross sections in Brewer and Dobson retrieval algorithms, Atmos. Chem. Phys., 14, 1635–1648, https://doi.org/10.5194/acp-14-1635-2014, 2014.

Rosenlof, K. H.: Seasonal cycle of the residual mean meridional circulation in the stratosphere, J. Geophys. Res., 100, 5173–5191, 1995.

Salawitch, R. J., McBride, L. A., Thompson, C. R., Fleming, E. L., McKenzie, R. L., Rosenlof, K. H., Doherty, S. J., and Fahey, D. W.: Twenty questions and answers about the ozone layer: 2022 update, in: Scientific Assessment of Ozone Depletion: 2022, p. 75, World Meteorological Organization, Geneva, Switzerland, 2023.

Santer, B. D., Wehner, M. F., Wigley, T. M. L., Sausen, R., Meehl, G. A., Taylor, K. E., Ammann, C., Arblaster, J., Washington, W. M., Boyle, J. S., and Brüggemann, W.: Contributions of anthropogenic and natural forcing to recent tropopause height changes, Science, 301, 479–483, https://doi.org/10.1126/science.1084123, 2003.

Schwartz, S. E. and Warneck, P.: Units for use in atmospheric chemistry, Pure Appl. Chem., 67, 1377–1406, 1995.

SCI-TEC Instruments Inc.: Brewer MKIV Spectrophotometer Operator's Manual, SCI-TEC Instruments Inc., Saskatoon, Canada, 1999.

https://doi.org/10.5194/egusphere-2025-2887
Preprint. Discussion started: 27 June 2025

Sen, P. K.: Estimates of the regression coefficient based on Kendall's tau, J. Am. Stat. Assoc., 63, 1379–1389, https://doi.org/10.1080/01621459.1968.10480934, 1968.

Serdyuchenko, A., Gorshelev, V., Weber, M., Chehade, W., and Burrows, J. P.: High spectral resolution ozone absorption crosssections – Part 2: Temperature dependence, Atmos. Meas. Tech., 7, 625–636, https://doi.org/10.5194/amt-7-625-2014, 2014.

Steinbrecht, W., Claude, H., Köhler, U., and Hoinka, K. P.: Correlations between tropopause height and total ozone: Implications for long-term changes, J. Geophys. Res.-Atmos., 103, 19183–19192, https://doi.org/10.1029/98JD01929, 1998.

Theil, H.: A rank-invariant method of linear and polynomial regression analysis, I, II, III, Proc. K. Ned. Akad. Wet., Ser. A, 53, 386–392, 521–525, 1397–1412, 1950.

United Nations Environment Programme (UNEP): Handbook for the Montreal Protocol on Substances that Deplete the Ozone Layer, Ozone Secretariat – UNEP, Nairobi, Kenya, https://ozone.unep.org/sites/default/files/Handbooks/MP-Handbook-2020-English.pdf, 2020.

Varotsos, C., Cartalis, C., Vlamakis, A., Tzanis, C., and Keramitsoglou, I.: The long-term coupling between column ozone and tropopause properties, J. Climate, 17, 3843–3854, https://doi.org/10.1175/1520-0442(2004)017<3843:TLTCBC>2.0.CO;2, 2004.

WMO: Guide to meteorological instruments and methods of observation, World Meteorological Organization, WMO – No 8, 7th Edn., Geneva, Switzerland, 2008.

World Meteorological Organization (WMO): Executive Summary. Scientific Assessment of Ozone Depletion: 2022, GAW Report No. 278, 56 pp., WMO, Geneva, Switzerland, https://ozone.unep.org/system/files/documents/Scientific-Assessment-of-Ozone-Depletion-2022-Executive-Summary.pdf, 2022.